CHINESE OPTICS LETTERS

Vol. 19, No. 8 | August 2021

Near-infrared lasing and tunable upconversion from femtosecond laser inscribed Nd,Gd:CaF_2 waveguides

Ruonan Li (李若男)[1], Lifei Sun (孙丽菲)[1], Yangjian Cai (蔡阳健)[1*], Yingying Ren (任莹莹)[1**], Hongliang Liu (刘洪亮)[2], Mark D. Mackenzie[3], and Ajoy K. Kar[3]

[1] Center of Light Manipulations and Applications & Shandong Provincial Key Laboratory of Optics and Photonic Device, School of Physics and Electronics, Shandong Normal University, Jinan 250014, China

[2] Institute of Modern Optics, Nankai University, Tianjin 300350, China

[3] Institute of Photonics and Quantum Sciences, Heriot-Watt University, Edinburgh EH14 4AS, UK

*Corresponding author: yangjiancai@sdnu.edu.cn

**Corresponding author: ryywly@sdnu.edu.cn

Received October 5, 2020 | Accepted December 30, 2020 | Posted Online April 22, 2021

Optical channel waveguides with depressed cladding configurations have been produced in Nd,Gd:CaF_2 laser crystals by using ultrafast laser inscription. Waveguide properties are investigated in terms of guiding behaviors and localized laser-induced lattice damages. Under an optical pump of 808 nm light, continuous-wave waveguide lasing at 1.06 μm is achieved, with a single-mode operation and a minimum lasing threshold of 98.8 mW. Furthermore, the visible emissions of Nd^{3+} with short wavelengths ranging from 415 nm to 550 nm and long wavelengths from 550 nm to 625 nm are observed upon 808 nm laser excitation via the up-converted process. The intensity ratios of two wavelength ranges are proved to be tunable through changing the pumping polarizations.

Keywords: femtosecond laser inscription; optical waveguide; CaF_2 crystal; laser; upconversion.
DOI: 10.3788/COL202119.081301

1. Introduction

Miniature laser devices that are constructed based on solid-state waveguide (WG) structures are gaining scientific and industrial interests owing to their hybrid functionality, highly compact platform, and inherent robustness. Moreover, benefiting from their small footprints, WG structures exhibit the ability of maintaining small spot sizes and hence high intra-cavity intensities, offering the attributes of reduced pump power threshold, high optical gain, and efficient lasing performance[1–4]. Ever since the pioneering report on laser operation of a glass WG in 1961[5], the merits of such a laser source have been highlighted in a broad spectrum of waveguiding platforms, and their applications range from the visible wavelength to the mid-infrared operating at the continuous wave (cw) and pulsed regimes[6–10].

With proper optical pumping, visible light trace may appear in the crystal, especially in the case of Ln^{3+}-doped crystals. Such a phenomenon is the so-called nonlinear anti-Stokes upconversion (UC) resulting from excited-state absorption (ESA) and/or from another kind of UC process that brings the excitation into the high-lying energy levels[11]. Although such phenomena, for most traditional laser devices that rely on the down-conversion mechanism, are drawbacks that degrade laser performance, the UC technology has rapidly progressed due to its unique advantages in advancing diverse applications such as high-level security fields[12], solar cell development[13,14], biological imaging[15], novel wavelength generation, and visible laser emission[16,17]. Combining these characteristics with the advances of WG architectures could trigger interests in their use for a broad range of integrated photonic applications[18–20].

The past decade saw the tremendous progress of femtosecond (fs) laser inscription (FLI) as a flexible, versatile, and relatively low-cost technology for WG fabrication in a wide range of transparent optical materials[3,21–24]. The intrinsic mechanism considered to be responsible for WG formation is the modification of the refractive index (RI) induced by the nonlinear photoionization processes of the light–matter interaction that occurs at the laser focus. This method works particularly well with optical crystals, and numerous WG structures have been proposed based on the single-line, double-line, and depressed cladding designs[3]. A depressed cladding structure consists of an unmodified core surrounded by a number of fs-laser-induced low-index tracks. Such geometries, which were first proposed, to the best of our knowledge, by Okhrimchuk *et al.* in Nd:$Y_3Al_5O_{12}$ (Nd:YAG)[25], have been proved to be superior to their counterparts, particularly in terms of flexible cross

© 2021 Chinese Optics Letters

sections (in both shape and size) and polarization-independent guidance. Up to now, WGs based on cladding configurations have been realized in crystals such as YAG and yttrium calcium oxyborate (YCOB) for WG lasers and nonlinear optics applications[20,26–28].

CaF_2 crystals, co-doped with Nd^{3+} ions and nonactive ions (such as Gd^{3+} and Y^{3+}), have received considerable attention. The introduction of nonactive ions has proven to be an effective method to suppress the formation of Nd^{2+} ions, therefore, enhancing the fluorescence quantum efficiency[20,29–32]. The extensive studies on these materials are mainly motivated by a number of salient features, including high segregation coefficient allowing large concentrations of rare-earth ions, broad absorption spectral bandwidth making them excellent for direct diode-pumped laser operation, and broad gain bandwidth raising the prospect of developing ultra-short pulsed laser sources.

In this work, we report on the fabrication of depressed cladding WGs in Nd,Gd:CaF_2 crystals by using FLI. The single-mode WG lasers at 1.06 μm have been realized along both of the transverse polarizations. In the guiding regions, visible UC of Nd^{3+} ions with two wavelength ranges possessing tunable intensity ratios is reported. This is, to the best of our knowledge, the first report on WG lasers and UC in this material.

2. Experimental Details

The surfaces and end-facets of the Nd,Gd:CaF_2 crystal (2.0% Nd^{3+}-ions and 5.0% Gd^{3+}-ions, atomic fraction) used in this work are polished to an optical quality. Cladding WGs are fabricated with an ultrafast Yb-doped fiber master-oscillator power amplifier laser (IMRA FCPA μ-Jewel D400) that delivers 360 fs pulses with 500 kHz repetition rate. The central wavelength is 1047 nm. The laser beam is circularly polarized and focused by a 0.4 numerical aperture (NA) aspheric lens into the substrate. The substrate is translated perpendicular to the laser beam axis at a speed of 20 mm/s. The average laser power deposited on the sample is finely controlled and varied from 160 mW to 100 mW with a step of 20 mW, which corresponds to pulse energy changing from 320 nJ to 200 nJ with a step of 40 nJ. Under these conditions, 16 tubular claddings, of 35 μm to 20 μm diameters, are inscribed with the center around 100 μm below the polished top surface (10 mm × 10 mm). In order to enhance the laser-induced RI modification, the scanning process is repeated with three overlapping scans for each track.

To investigate the guiding behavior of the WGs, a linearly polarized 633 nm diode laser is coupled into the WG core regions through a typical end-face coupling arrangement. The propagation loss α is estimated by the equation

$$P_{\text{out}} = P_{\text{in}} \cdot (1-R)^2 \cdot e^{-\alpha L} \cdot T,$$

where R is the Fresnel reflection coefficient, L denotes the length of the WG, and T is related to the mismatch between the pump beam mode and WG mode, which, for single-mode WGs, can be expressed as

$$T = \left(\frac{2\omega_1\omega_2}{\omega_1^2+\omega_2^2}\right)^2,$$

where ω_1 and ω_2 are the mode widths of the WG and pump beam, respectively. The RI contrast is roughly approximated by using the formula

$$\Delta n = \frac{\sin^2\theta_m}{n},$$

in which θ_m is the maximum incident angle, where no change of the transmitted power is occurring, and n is the RI of the substrate.

A fiber-coupled confocal microscope (alpha300 R, WITec GmBH) is used to investigate the confocal micro-photoluminescence (μ-PL) properties of the fabricated WG1 as a representative. A 532 nm excitation laser is focused to a diffraction-limited spot size onto the WG cross section by using a 50× microscope objective with NA = 0.55, exciting the transition of Nd^{3+} ions from the ground state $^4I_{9/2}$ up to the $^2G_{3/2}$ excited state. The backscattered μ-PL corresponding to the $^4F_{3/4}$ to $^4I_{9/2}$ emission band is dispersed by a 600 mm focal length spectrometer with 300 grooves/mm grating (UHTS 600).

For laser characterization experiments, a Ti:sapphire cw laser (Coherent MBR 110, USA) generating a linearly polarized beam at 808 nm is employed as the pump source. A half-wave plate is used to control the polarization of the pump laser beam, so that the lasing properties in both transverse electric (TE) and transverse magnetic (TM) polarizations can be investigated. The pump beam is coupled into the WGs with a convex lens (f = 50.8 mm), which gives a diffraction-limited pump spot size of about 35 μm ($1/e^2$ intensity diameter) at the focus, ensuring good overlapping between the pump mode and the guided modes. The output beam was collected by a 20× microscope objective. Two dielectric mirrors are butt-coupled to the polished end-facets to form a Fabry–Perot cavity for the 1.06 μm WG laser emission. After being separated from the residual pump, the laser emissions from the WG are detected.

Similarly, the UC emission is excited with the polarized 808 nm Ti:sapphire laser. The same end-coupling system as for the WG laser characterization is utilized, except no cavity mirror is applied here.

3. Results and Discussion

Figure 1(a) shows the cross-sectional images of the produced WGs observed with an optical microscope. Zoomed-in images of WGs fabricated with 320 nJ pulse energy and with diameters of 35 μm (WG1), 30 μm (WG2), 25 μm (WG3), and 20 μm (WG4) are shown in Figs. 1(b)–1(e), which reveal distinct guiding boundaries without any cracks in the guiding cores or in the bulk. The intact cores are expected to preserve comparable optical properties to the substrate and, hence, possess potentials for laser generation.

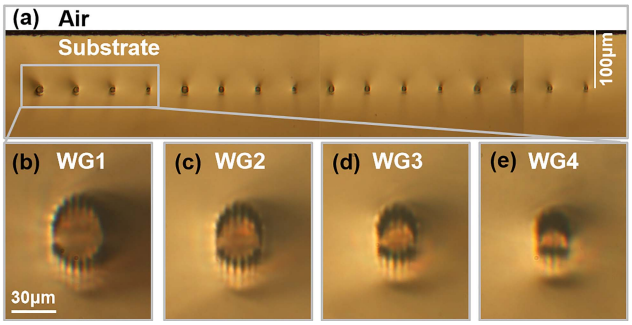

Fig. 1. (a) Microscopic image of the end-facet of the Nd,Gd:CaF_2 sample with 16 cladding WGs deeply embedded beneath the surface. (b)–(e) The cross sections of WG1–WG4.

Figure 2(a) displays the output intensity (normalized) distributions measured under TM polarization. It is worthy to point out that these WGs could support arbitrary polarizations, and the mode distributions do not exhibit significant polarization dependence as a result of the symmetric morphology of the cladding structures. Strong optical confinements are obtained from all WGs. Particularly, single-mode guidance is observed from structures with a diameter of 20 μm due to the relatively small guiding areas. Furthermore, a WG produced with 200 nJ laser energy and 25 μm diameter, although possessing a larger size, also supports single-mode guidance owing to the low inscription energy that induces small RI modification. The propagation losses of the WG are shown in Fig. 2(b), which reveals that, in general, reduced propagation losses are obtained with larger guiding cores and higher irradiated laser energies. The minimum value is estimated to be around 0.87 dB/cm for WG1, with negligible differences for TE and TM polarizations. Hence, all of the results described hereafter are implemented with WG1. The RI contrast of WG1 is estimated to be around 7×10^{-3}.

Figure 3(a) shows the μ-PL emission spectra obtained from the unmodified bulk region, WG area, and laser-induced track, corresponding to the spots A, B, and C in the inset, respectively. It can be observed that, at the center of the damage track, the μ-PL intensity suffers from a strong quenching, while spectra from both WG and bulk are identical without any variance of spectral distribution and intensity. In order to obtain the detailed modification of μ-PL properties, the spatial dependences of the emitted intensity, peak position, and line width (FWHM) of the 867 nm line are investigated, as displayed in Figs. 3(b)–3(d), respectively. Meanwhile, for easy visualization and comparison, Figs. 3(e)–3(g) show the one-dimensional (1D) profiles corresponding to the positions indicated by the dashed lines in the inset of Fig. 3(a). It is clear that obvious intensity reduction in company with broadening of the emission line occurred at the filament locations, indicating high density of lattice defects and imperfections in these areas. In addition, blue shift of the μ-PL emission spectra in the filaments can be observed, which is aroused by lattice damages and expansive stress. These results coincide well with that obtained from WG structures in $Pr:CaF_2$ crystals fabricated by FLI[33]. At the same time,

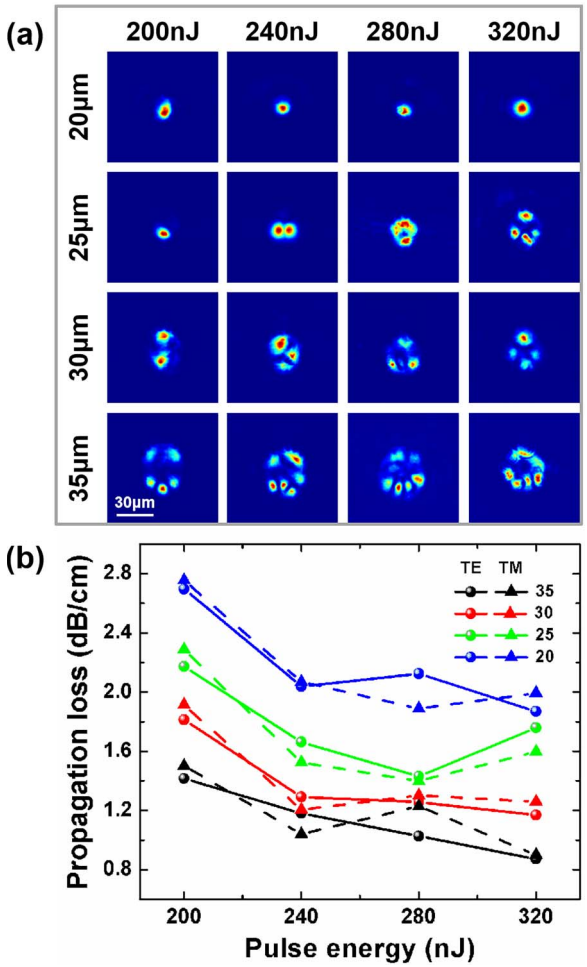

Fig. 2. (a) Mode intensity distributions from the fabricated cladding WGs at 633 nm under TM polarization. (b) Propagation losses of WGs obtained under both TM and TE polarizations.

identical μ-PL intensity, peak position, and FWHM profiles are observed in the WG volumes and the bulk, which means that the core guiding region is composed by a high-quality unirradiated crystalline network, which preserves the original properties for laser and nonlinear optics applications.

The laser output power from WG1 versus incident power is measured by using output couplers with 9% and 70% reflectance, the results of which are shown in Figs. 4(a) and 4(b). As can be seen, by using the 9% output coupler, the WG laser system exhibits a lasing threshold as low as 98.8 mW and 114.2 mW at TM and TE polarizations, respectively, while higher slope efficiency of around 13% is obtained with the 70% coupler, which leads to a maximum output power of 35 mW with 440 mW incident pump power, corresponding to an optical-to-optical conversion efficiency of around 8%. One can expect better lasing performance by further optimizing the WG structures and decreasing their propagation losses through, for example, increasing scan times for each track or enlarging the WG diameters. Figure 4(c) shows the generated WG laser spectrum, centered at 1059.91 nm with an FWHM of 6.7 nm. The inset of Fig. 4(c) demonstrates the lasing mode

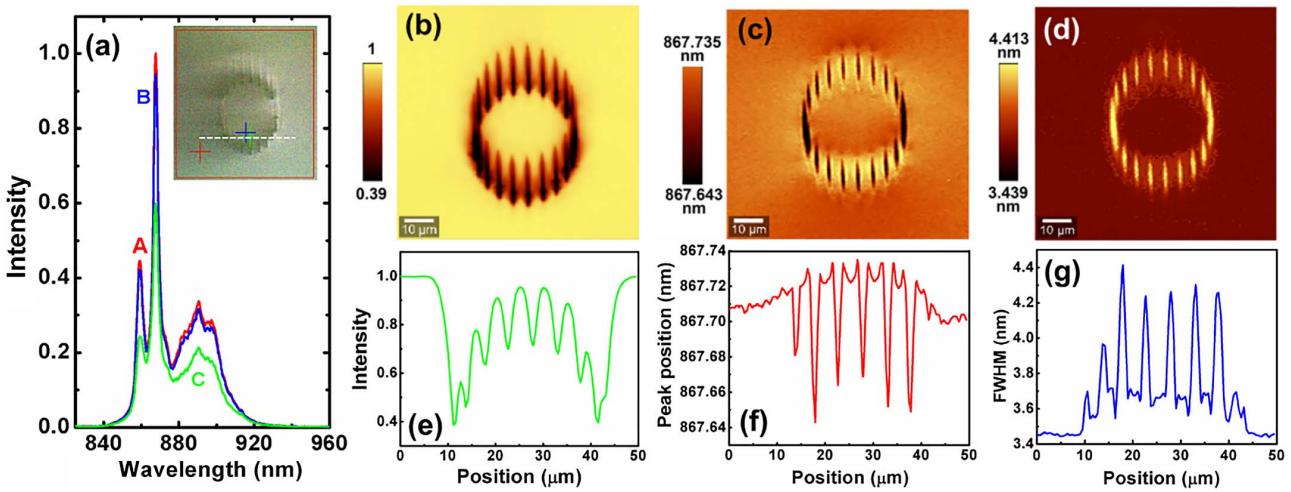

Fig. 3. (a) The room temperature μ-PL emission spectra of Nd^{3+} ions obtained from the WG area (blue), the filament (green), and the bulk of Nd,Gd:CaF_2 crystals (red). The inset of (a) shows the cross section of WG1. The spatial two-dimensional (2D) distributions of (b) intensity, (c) peak shift, and (d) FWHM of 867 nm emission line obtained from the WG cross section. 1D distributions of (e) the emitted intensity, (f) energy shift, and (g) FWHM corresponding to the regions indicated by dashed lines in the inset of (a).

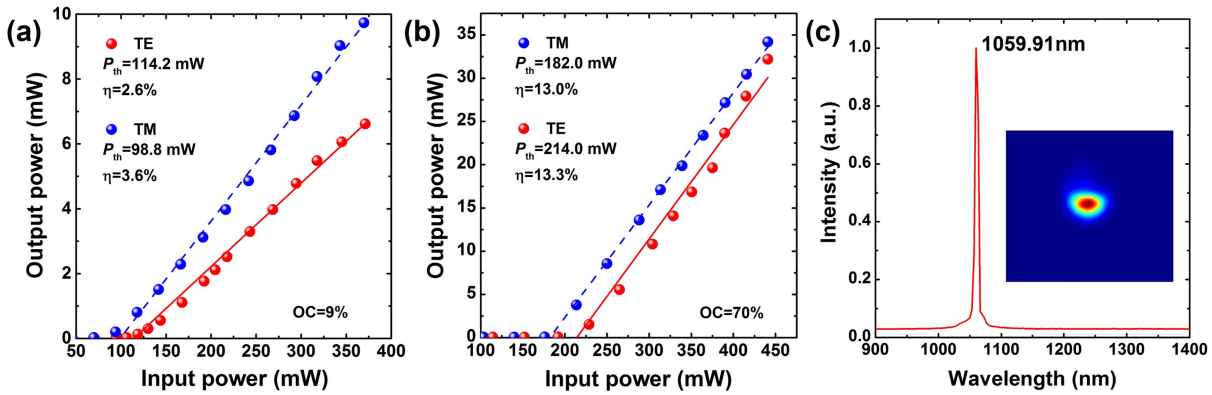

Fig. 4. cw WG laser output power as a function of the input pump power with (a) 9% and (b) 70% output coupler. (c) Spectrum of WG laser at 1059.91 nm. The inset shows the spatial intensity distribution of the output laser with a single-mode profile.

emitted from WG1, confirming the single-mode operation at 1.06 μm, which is an intriguing feature of this laser device for its applications.

Figures 5(a) and 5(b) exhibit photographs of visible UC emissions observed in WG1 and the bulk area, from which strong confinement of luminescence in the WG can be observed, while clear intensity quenching occurred in the bulk. Figures 5(c) and 5(d) show the UC luminescence spectra obtained under increasing excitation power. When excited with the TE polarized laser, as shown in Fig. 5(a), the luminescence consists of a short-wavelength range (SWR) from 415 nm to 550 nm and a long-wavelength range (LWR) of 550 nm to 625 nm, with each waveband splitting into several subpeaks. In contrast, with TM polarized laser excitation, the wavelength regions preserve the original positions, whereas LWR is nearly absent, leading to a large intensity ratio of SWR and LWR components. A key feature of the spectrum, under both TE and TM polarized laser excitations, is the steady increase of the luminescence emission with the increasing excitation power.

In order to investigate the effect of polarization of the excitation laser on the UC, the generated luminescence spectra are measured as the half-wave plate rotating from angles of 0° to 90° under the same coupling conditions, corresponding to polarization varying from TE to TM and then back to TE. The results are shown in Fig. 6(a), further confirming the strong polarization dependence of the luminescence spectra. To get a clear picture of the competition between SWR and LWR, we focus on two stationary peaks at 485 nm and 585 nm. In Figs. 6(b) and 6(c), the experimentally determined luminescence intensities are shown as a function of the angles of the polarizer, which demonstrate strong periodic dependence of each peak on the polarization. The intensity ratios between the two peaks are

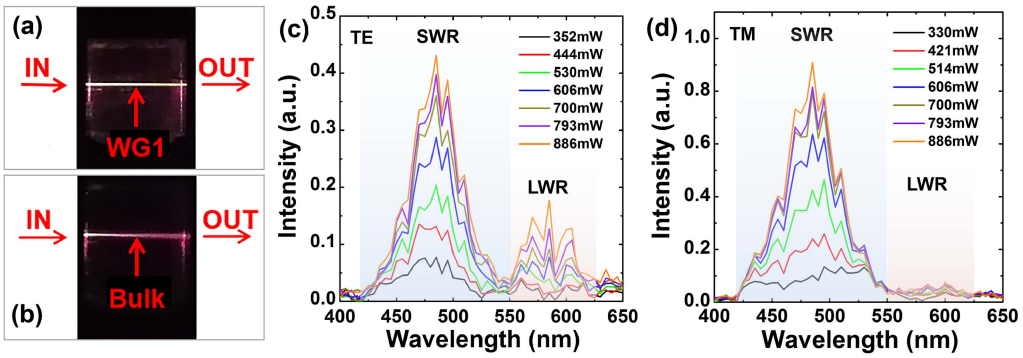

Fig. 5. Photographs of visible UC luminescence generated from (a) WG1 and (b) the bulk. UC spectra obtained from WG1 under (c) TE and (d) TM polarizations with varying excitation powers.

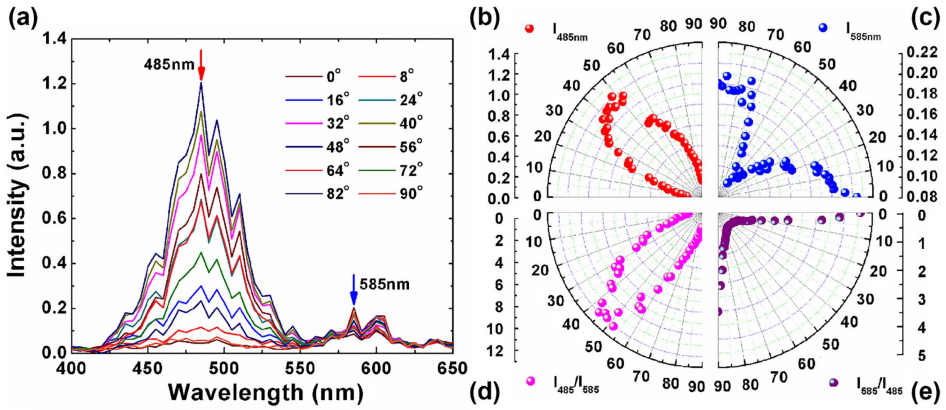

Fig. 6. (a) UC spectra from WG1 obtained with a rotating half-wave plate. Luminescence intensities of emission lines centered at (b) 485 nm and (c) 585 nm as a function of the angles of the polarizer. The intensity ratios of (d) I_{485}/I_{585} and (e) I_{585}/I_{485} as a function of the angles of the polarizer.

determined and presented in Figs. 6(d) and 6(e). The maximum values of the spectral intensity ratio of I_{485}/I_{585} and $I_{585}/I_{485}$are found to be 12.16 and 4.76, respectively. The variation of UC spectra, in a first-order approximation, can be interpreted from the perspective of ESA, whose cross sections show polarized difference in Nd^{3+}-doped crystalline materials[34]. Additionally, it is also noted that the higher luminescence intensity of SWR can be obtained rather than that of LWR, indicating larger quantum yields of Nd^{3+} ions for up-converted emissions in SWR. Such a WG system provides us with the possibility for the construction of UC WG lasers and controllable wavelengths of the UC luminescence.

4. Conclusion

Cladding WGs are fabricated in a Nd,Gd:CaF_2 crystal by using FLI under different inscription conditions. Propagation loss as low as 0.87 dB/cm is obtained. WG lasers are realized with low lasing thresholds and single-mode profiles. UC luminescences of Nd^{3+}-ions consisting of SWR from 415 nm to 550 nm and LWR from 550 nm to 625 nm are achieved with tunable intensity ratios of two ranges. These results make the WGs fabricated in this work promising for constructing miniature devices and integrated optical circuits for the 1 μm and visible optical applications.

Acknowledgement

This work was supported by the National Key Research and Development Project of China (No. 2019YFA0705000), the National Natural Science Foundation of China (NSFC) (Nos. 11874243, 11525418, 91750201, and 11974218), the Innovation Group of Jinan (No. 2018GXRC010), and the Local Science and Technology Development Project of the Central Government (No. YDZX20203700001766).

References

1. C. Grivas, "Optically pumped planar waveguide lasers: part II: gain media, laser systems, and applications," Prog. Quantum Electron. **45–46**, 3 (2016).
2. Y. C. Jia and F. Chen, "Compact solid-state waveguide lasers operating in the pulsed regime: a review," Chin. Opt. Lett. **17**, 012302 (2019).
3. F. Chen and J. R. Vázquez de Aldana, "Optical waveguides in crystalline dielectric materials produced by femtosecond-laser micromachining," Laser Photon. Rev. **8**, 251 (2014).

4. F. Chen, "Micro- and submicrometric waveguiding structures in optical crystals produced by ion beams for photonic applications," Laser Photon. Rev. **6**, 622 (2012).
5. J. Leute, N. Huntemann, B. Lipphardt, C. Tamm, P. B. R. Nisbet-Jones, S. A. King, R. M. Godun, J. M. Jones, H. S. Margolis, P. B. Whibberley, A. Wallin, M. Merimaa, P. Gill, and E. Peik, "Frequency comparison of $^{171}Yb^{+}$ ion optical clocks at PTB and NPL via GPS PPP," IEEE. Trans. Ultrason. Ferr. **63**, 981 (2016).
6. C. Kränkel, D. T. Marzahl, F. Moglia, G. Huber, and P. W. Metz, "Out of the blue: semiconductor laser pumped visible rare-earth doped lasers," Laser Photon. Rev. **10**, 548 (2016).
7. Y. Y. Ren, C. Cheng, Y. C. Jia, Y. Jiao, D. W. Li, M. D. Mackenzie, A. K. Kar, and F. Chen, "Switchable single-dual-wavelength Yb,Na:CaF_2 waveguide lasers operating in continuous-wave and pulsed regimes," Opt. Mater. Express **8**, 1633 (2018).
8. C. Grivas, C. Corbari, and G. Brambilla, "Recent progress in continuous-wave Ti:sapphire waveguide lasers," Proc. SPIE **8988**, 898808 (2014).
9. Y. Y. Ren, G. Brown, R. Mary, G. Demetriou, D. Popa, F. Torrisi, A. C. Ferrari, F. Chen, and A. K. Kar, "7.8-GHz graphene-based 2-μm monolithic waveguide laser," IEEE. J. Set. Top. Quantum Electron. **21**, 1602106 (2015).
10. S. A. Mcdaniel, A. Lancaster, J. W. Evans, A. K. Kar, and G. Cook, "Power scaling of ultrafast laser inscribed waveguide lasers in chromium and iron doped zinc selenide," Opt. Express **24**, 3502 (2016).
11. J. E. Moffact, G. Tsiminis, E. Klantsataya, T. J. de Prinse, D. Ottaway, and N. A. Spooner, "A practical review of shorter than excitation wavelength light emission processes," Appl. Spectrosc. Rev. **55**, 327 (2019).
12. W. J. Yao, Q. Y. Tian, and W. Wu, "Tunable emissions of upconversion fluorescence for security applications," Adv. Opt. Mater. **7**, 1801171 (2019).
13. D. Y. Li, H. Ågren, and G. Y. Chen, "Near infrared harvesting dye-sensitized solar cells enabled by rare-earth upconversion materials," Dalton. Trans. **47**, 8526 (2018).
14. Y. Qiao, S. H. Li, W. H. Liu, M. Q. Ran, H. F. Lu, and Y. P. Yang, "Recent advances of rare-earth ion doped luminescent nanomaterials in perovskite solar cells," Nanomaterials **8**, 43 (2018).
15. Y. Choi, S. H. Baek, S. J. Chang, Y. Song, R. Rafique, and K. T. Lee, "Synthesis of upconversion nanoparticles conjugated with graphene oxide quantum dots and their use against cancer cell imaging and photodynamic therapy," Biosens. Bioelectron. **93**, 267 (2017).
16. A. Fernandez-Bravo, K. Y. Yao, E. S. Barnard, N. J. Borys, E. S. Levy, B. Tian, C. A. Tajon, L. Moretti, M. V. Altoe, S. Aloni, K. Beketayev, F. Scotognella, B. E. Cohen, E. M. Chan, and P. J. Schuck, "Continuous-wave upconverting nanoparticle microlasers," Nat. Nanotechnol. **13**, 572 (2018).
17. B. Guzelturk, Y. Kelestemur, K. Gungor, A. Yeltik, M. Z. Akgul, Y. Wang, R. Chen, C. Dang, H. Sun, and H. V. Demir, "Stable and low-threshold optical gain in CdSe/CdS quantum dots: an all colloidal frequency upconverted laser," Adv. Mater. **27**, 2741 (2015).
18. Z. B. Li, J. X. Yang, M. Shi, and L. Yang, "Upconversion luminescence of graphene oxide through hybrid waveguide," J. Phys. Chem. C **122**, 16866 (2018).
19. J. M. Lv, X. T. Hao, and F. Chen, "Green up-conversion and near-infrared luminescence of femtosecond-laser-written waveguides in Er^{3+}, MgO co-doped nearly stoichiometric $LiNbO_3$ crystal," Opt. Express **24**, 25482 (2016).
20. L. M. Zhang, T. Y. Guo, Y. Y. Ren, Y. J. Cai, M. D. Mackenzie, A. K. Kar, and Y. C. Yao, "Cooperative up-converted luminescence in Yb,Na:CaF_2 cladding waveguides by femtosecond laser inscription," Opt. Commun. **441**, 8 (2019).
21. R. Osellame, H. Hoekstra, G. Cerullo, and M. Pollnau, "Femtosecond laser microstructuring: an enabling tool for optofluidic lab-on-chips," Laser Photon. Rev. **5**, 442 (2011).
22. D. Choudhury, J. R. Macdonald, and A. K. Kar, "Ultrafast laser inscription: perspectives on future integrated applications," Laser Photon. Rev. **8**, 827 (2014).
23. K. Sugioka and Y. Cheng, "Ultrafast lasers-reliable tools for advanced materials processing," Light Sci. Appl. **3**, e149 (2014).
24. D. Z. Tan, K. N. Sharafudeen, Y. Z. Yue, and J. R. Qiu, "Femtosecond laser induced phenomena in transparent solid materials: fundamentals and applications," Prog. Mater. Sci. **76**, 154 (2016).
25. A. G. Okhrimchuk, A. V. Shestakov, I. Khrushchev, and J. Mitchell, "Depressed cladding, buried waveguide laser formed in a YAG: Nd^{3+}crystal by femtosecond laser writing," Opt. Lett. **30**, 2248 (2005).
26. Y. Y. Ren, G. Brown, A. Ródenas, S. Beecher, F. Chen, and A. K. Kar, "Mid-infrared waveguide lasers in rare-earth-doped YAG," Opt. Lett. **37**, 3339 (2012).
27. Y. C. Jia, R. Y. He, J. R. Vázquez de Aldana, H. L. Liu, and F. Chen, "Femtosecond laser direct writing of few-mode depressed-cladding waveguide lasers," Opt. Express **27**, 30941 (2019).
28. Y. Y. Ren, F. Chen, and J. R. Vázquez de Aldana, "Near-infrared lasers and self-frequency-doubling in Nd:YCOB cladding waveguides," Opt. Express **21**, 11562 (2013).
29. J. Du, X. Y. Liang, Y. G. Wang, L. B. Su, W. W. Feng, E. W. Dai, Z. Z. Xu, and J. Xu, "1 ps passively mode-locked laser operation of Na,Yb:CaF_2 crystal," Opt. Express **13**, 7970 (2005).
30. L. B. Su, J. Xu, H. J. Li, W. Q. Yang, Z. Q. Zhao, J. L. Si, Y. J. Dong, and G. Q. Zhou, "Codoping Na^{+} to modulate the spectroscopy and photoluminescence properties of Yb^{3+} in CaF_2 laser crystal," Opt. Lett. **30**, 1003 (2005).
31. J. L. Doualan, L. B. Su, G. Brasse, A. Benayad, V. Menard, Y. Y. Zhan, A. Braud, P. Camy, J. Xu, and R. Moncorgé, "Improvement of infrared laser properties of Nd:CaF_2 crystals via codoping with Y^{3+} and Lu^{3+} buffer ions," J. Opt. Soc. Amer. B **30**, 3018 (2013).
32. S. Y. Pang, F. K. Ma, H. Yu, X. B. Qian, D. P. Jiang, Y. J. Wu, F. Zhang, J. Liu, J. Y. Xu, and L. B. Su, "Highly efficient continuous-wave laser operation of LD-pumped Nd,Gd:CaF_2 and Nd,Y:CaF_2 crystals," Laser Phys. Lett. **15**, 055802 (2018).
33. T. Y. Guo, R. N. Li, L. F. Sun, Y. J. Cai, Y. Y. Ren, Y. C. Yao, M. D. Mackenzie, and A. K. Kar, "Femtosecond laser inscribed Pr:CaF_2 waveguides: micro-spectroscopy characterizations and refractive index reconstruction," Opt. Commun. **461**, 125243 (2020).
34. Y. Guyot, H. Manaa, J. Y. Rivoire, R. Moncorgé, N. Garnier, E. Descroix, M. Bon, and P. Laporte, "Excited-state-absorption and upconversion studies of Nd^{3+}-doped single crystals $Y_3Al_5O_{12}$, $YLiF_4$, and $LaMgAl_{11}O_{19}$," Phys. Rev. B **51**, 784 (1995).